DEM SIMULATION OF RAILWAY BALLAST USING POLYHEDRAL ELEMENTAL SHAPES

JAN ELIÁŠ

Brno University of Technology, Faculty of Civil Engineering,Institute of Structural Mechanics
Veveří 331/95, Brno, 602 00, Czech Republic
elias.j@fce.vutbr.cz, http://www.fce.vutbr.cz/STM/elias.j

Key words: ballast, DEM, polyhedral shape, oedometer test

Abstract. Modelling of railway ballast response using Discrete Element Method with polyhedral shape of grains is presented. The convex polyhedrons are generated pseudo-randomly via Voronoi tessellation. Inter-particle contact is based on calculation of intersecting (polyhedral) volume. Large oedometric test is simulated using this model and results are compared to an experimental data from literature.

1 INTRODUCTION

Discrete Element Method (DEM) has been successfully applied to many engineering problems. In most cases, the simplest spherical elemental shapes are used. However, it has been reported that the particle shape has a strong influence on resulting behavior of the particle assembly. Therefore, more realistic shapes are being considered. This is often achieved by clumping spheres into some more complex aggregations [5]. Such a method has an advantage in simplicity and computational speed. Another approach lies in direct implementation of some non-spherical elements. A contact detection algorithm and an algorithm for determination of contact forces between the non-spherical particles must be developed. Examples can be found in Bathurst and Rothenburg [1] for elliptical shapes, Song et al. [20] for tablet shapes or in Nezami et al. [18] for polyhedral shapes.

One can find also papers comparing these two methods of representation of realistic shapes. In Szarf et al. [21], response of polygonal particles is compared to response of spherical clumps. The same in 3D is shown in Höhner et al. [8] for polyhedrons and spherical clumps.

In case of convex polyhedrons, a technique developed by Cundall [4, 7] called *common plane method* is often used. It replaces contact between two polyhedrons by two plane-polyhedron contacts. This method was further improved by fast determination of the common plane [16, 17]. Somehow different approach was developed in Boon et al. [2]. Instead of the common plane method, their contact forces are derived via inner "potential particles".

There have been several attempts to simulate railway ballast using DEM. The reported results seems to be promising. The ballast particles are represented either by spherical clumps [13], polygons [19] or polyhedrons [9]. An important part of the ballast behavior is its crushing. The crushing might be modeled as splitting of clumps [13] or by replacing the damaged particle by two or more smaller particles [14].

In this contribution, we present another possible way how to estimate contact forces between two polyhedrons. The repulsive force linearly increases with a volume of a polyhedrons intersection. The contact normal direction (in which the repulsive force acts) is estimated by the least square fitting of a polyhedron surfaces intersection by a tangent plane. The contact shear force is evaluated by the standard incremental algorithm with Coulomb friction.

The polyhedral contact model is developed to be used for railway ballast simulations. Crushing is not presented in the contribution, but it can (and it will) be simply introduced by cutting the polyhedrons into smaller ones. The shape of polyhedral ballast particles is generated by Voronoi tessellation on randomly placed points. It is therefore random, but its overall size as well as its aspect ratio can be controlled.

The model is applied to simulation of a large oedometric test and results are compared to an experimental data taken from literature.

Algorithms presented in the contribution were implemented into the open source DEM software YADE [23, 11]. Manipulation with polyhedrons as well as computation of convex hulls and least square fitting by plane is done via open source software CGAL [10, 3].

2   RANDOMLY GENERATED POLYHEDRAL SHAPES

The polyhedrons are generated by Voronoi tessellation on pseudo-randomly placed nuclei. Initially, some volume (in our case of size $5 \times 5 \times 5$ units) is filled by nuclei with minimal mutual distance $d_{\min}$. Starting with nucleus $\boldsymbol{C}_0 = (0,0,0)$ in the center of the volume, other nuclei with random coordinates are accepted if their distance to all previously placed nuclei exceeds $l_{\min}$. This is repeated until no nucleus is accepted for 500 subsequent trials. Restricting distance $l_{\min}$ is set to 0.75 units, because then the average distance between points is close to 1 unit. Voronoi tessellation is performed and the Voronoi cell associated with the central nucleus $\boldsymbol{C}_0$ is extracted and used as a basic polyhedral shape.

This Voronoi cell is further rescaled in all three directions by factor $\boldsymbol{s} = (s_x, s_y, s_z)$. Every vertex $\bar{\boldsymbol{x}}$ of the basic polyhedron is therefore transformed by the scaling vector: $\boldsymbol{x} = (\bar{x}s_x, \bar{y}s_y, \bar{z}s_z)$. The final grain shape is then given by vertices $\boldsymbol{x}$. Because the scaling procedure scales along axes x, y and z, the final polyhedron is also randomly rotated to prevent directional bias.

Volume, centroid and inertia of the polyhedral particle is calculated through dividing its volume into tetrahedrons. Contributions of tetrahedrons to each of the wanted quantity are found using analytical formulas from Tonon [22]. Figure 1 shows some resulting random polyhedrons. Three scaling aspect ratios are considered in the figure.
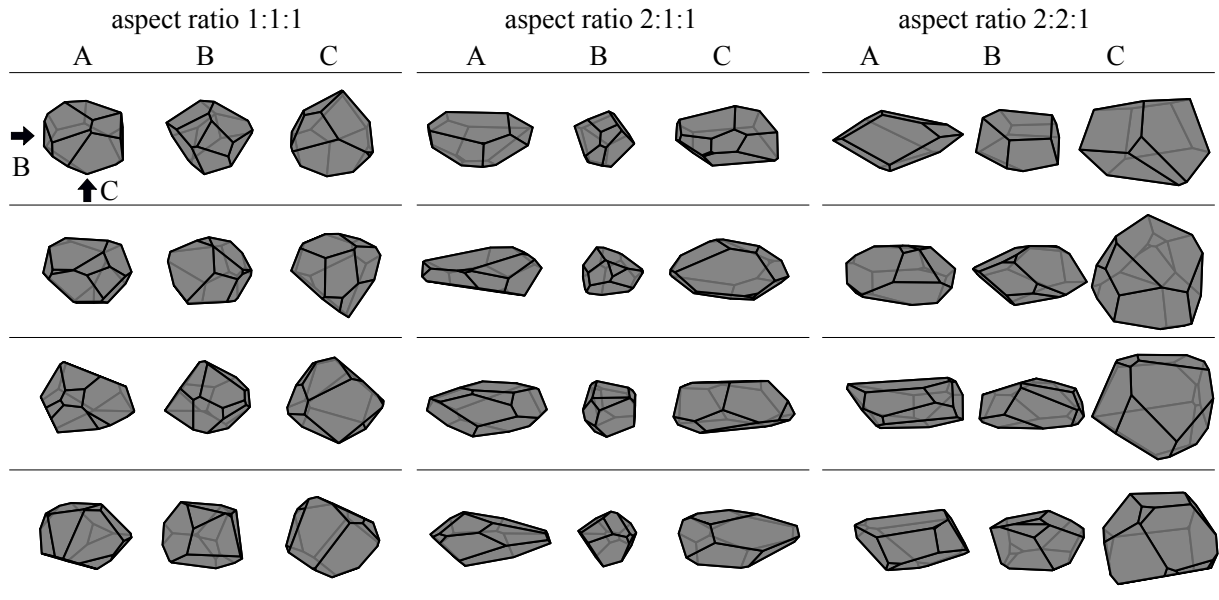
Figure 1: Randomly shaped grains generated via Voronoi tessellation. Three variants differs by prescribing different scaling factors along x, y and z axes. Each polyhedral grain is showed in front (A), side (B) and bottom (C) view.

3   CONTACT BETWEEN TWO POLYHEDRONS

In every step, there is a loop detecting all possible contacts between polyhedral elements. This is simply done through creation of bounding boxes around every polyhedron and detection of overlapping between the bounding boxes. Box overlapping exists if and only if bounding boxes overlap along all three axis. The problem is therefore reduced into triple overlap detection of segments in 1D.

3.1   Contact detection

If box overlapping is detected, one must check overlapping between polyhedrons $\mathcal{A}$ and $\mathcal{B}$. The polyhedrons are represented through set of oriented planes A_i that creates polyhedron facets

$$A_i(x, y, z) = n_x x + n_y y + n_z z + a = 0 \tag{1}$$

where $\boldsymbol{n} = (n_x,\, n_y,\, n_z)$ is the normal vector pointing outwards from the polyhedron and a is a constant determining position of the plane.

Overlapping is assumed until some separation plane is found. One should search for separation plane in a set that contains (i) facet planes A_i of the polyhedron $\mathcal{A}$; (ii) facet planes B_i of the polyhedron $\mathcal{B}$; and (iii) planes determined by one edge from $\mathcal{A}$ and another edge from $\mathcal{B}$. A loop over all these plane candidates is browsed. Every time, a trial separation plane that constitutes two halfspaces is constructed. All vertices from the first polyhedron $\mathcal{A}$ must lay at one halfspace whereas all vertices from second

polyhedron $\mathcal{B}$ must lay in the other halfspace. Whenever such condition is fulfilled, the separation plane is found and polyhedrons do not overlap. If the loop is finished without any separation plane found, there is a contact between polyhedrons.

To save computational time, one can store entities that defined the separation plane and in the next time step start with the trial separation plane using these entities with updated positions. Time savings can be gained also for polyhedrons previously in contact. One can simply check if the centroid of the intersection polyhedron c_I from the previous time step still lies in both polyhedrons with updated position and orientation. This is performed by a loop running through all the facet planes of both polyhedrons and checking that the centroid c_I is on the negative side of all those planes.

The procedure operates with a verification on which side of the plane some point x is. This can be determined by inserting the point x into the plane equation 1 and signum of the resulting value tells us in which halfspace the point lies.

3.2 Repulsive force

It is assumed, that the normal force acts at the centroid c_I of the intersection $\mathcal{I}$. Magnitude of the repulsive normal force $|\boldsymbol{F}_n|$ is determined from intersection volume V_I

$$|\boldsymbol{F}_n| = V_I k_n \tag{2}$$

where k_n [N/m³] is a material parameter called volumetric stiffness. A complication of such definition is evaluation of the intersection volume. This operation is computationally demanding. Here, we use the dual approach to find it [15, 6].

- Both of the intersecting polyhedrons are dualized. Facet planes (Eq. 1) from both polyhedrons are transformed into dual points $\widehat{A}_i$ and $\widehat{B}_i$.

$$\widehat{A}_i = (n_x/a, n_y/a, n_z/a) \tag{3}$$

- The convex hull of these dual points is found. Such convex hull is again a convex polyhedron determined by its oriented facet planes.

- The polyhedron in the dual space found in the previous step is dualized again using Eq. 3. These dual points are actually real points as we project them from the dual space into the real one.

- Finally, convex hull of points from the previous step gives us the intersecting convex polyhedral object $\mathcal{I}$.

Volume V_I and centroid c_I of the intersection is then easily found by dividing $\mathcal{I}$ into tetrahedrons as is done for the whole polyhedral particles.

The dualization algorithm requires that the origin must be inside the resulting intersection volume. One therefore needs to find some point inside both polyhedrons and translate
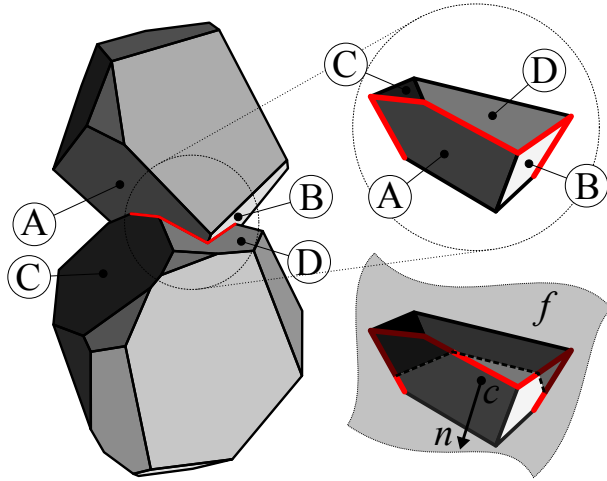
Figure 2: Two polyhedral particles in contact, intersecting polyhedron $\mathcal{I}$, centroid and normal direction.

the problem into a new coordinate system with origin at the common point before the dualization is started. For existing intersection, we use the intersection centroid $\boldsymbol{c}_I$ from the last time step (but only if it remains in both polyhedrons with updated positions). For new interactions, such point is found by searching for any facet-edge intersection.

Figure 2 shows two particles in contact and its polyhedral intersection.

3.3 Normal direction

Furthermore, we need to determine direction of the normal force $\boldsymbol{F}_n$. Motivated by 2D sketches, we decided to fit the polyhedra surfaces intersection by a plane f and set the normal direction to be perpendicular to that plane.

After finding the intersecting polyhedron, its facets are divided to those belonging originally to $\mathcal{A}$ polyhedron and to $\mathcal{B}$ polyhedron, respectively. Edges on the boundary between these two groups are then interpolated by a plane f with normal vector $\boldsymbol{n}$ using the least square fitting. The force $\boldsymbol{F}_n$ is then given by

$$\boldsymbol{F}_n = \boldsymbol{n}|\boldsymbol{F}_n|/|\boldsymbol{n}| \tag{4}$$

The boundary edges fitted by the normal plane f are showed in Fig. 2 in red color.

3.4 Shear force

Shear force $\boldsymbol{F}_s$ is calculated by standard incremental algorithm [23]. Shear force from the last time step is corrected for changes in the normal direction and for the rigid-body motion. Then, an additional shear displacement increment caused by mutual movements and rotations of polyhedrons $\Delta\boldsymbol{u}_s$ is calculated and the shear force is adjusted by increment

$$\Delta\boldsymbol{F}_s = \Delta\boldsymbol{u}_s k_s \tag{5}$$

where k_s [N/m] stands for shear stiffness of the material.

Standard Coulomb friction is applied. Therefore, whenever the shear force violates following condition

$$|F_s| \leq \varphi |\boldsymbol{F}_n| \tag{6}$$

it is reduced to fulfill equality in Eq. 6. Coefficient φ is called friction angle.

4 OEDOMETER TEST SIMULATION

4.1 Description of the experiment

We validated the proposed model by simulating a large oedometric test on railway ballast performed and published by Lim [12]. They tested several different ballasts, from which we chose variant A with ballast particle size in interval 37.5-50 mm. A steel cylinder of diameter 300 mm and depth 150 mm was filled by the ballast and vibrated on a vibration table with surcharge force 250 N. Then, it was loaded in compression up to force -1.5 MN (mean stress 21.2 MPa). Total duration of the experiment was about 40 minutes.

The same experiment was previously simulated in Lim and McDowell [13] using crushable sphere clumps. The loading time was shortened to approx. 0.4 s. The published results agrees with the experimental data except the initial part, because the vibration was not simulated.

4.2 DEM simulation

Initially, randomly shaped polyhedrons were generated at random positions in a cylinder of magnified depth 1 meter with no overlapping. This was done by sequential placing of trial polyhedrons that were rejected each time when any conflict with previously placed particles appeared. The polyhedrons then fall freely under 5 times magnified gravitational acceleration and reduced friction angle 0.1 radians. Both gravity and friction changes were done to increase compaction of the assembly. After reaching low unbalanced forces, all

Table 1: Material properties used in simulations.

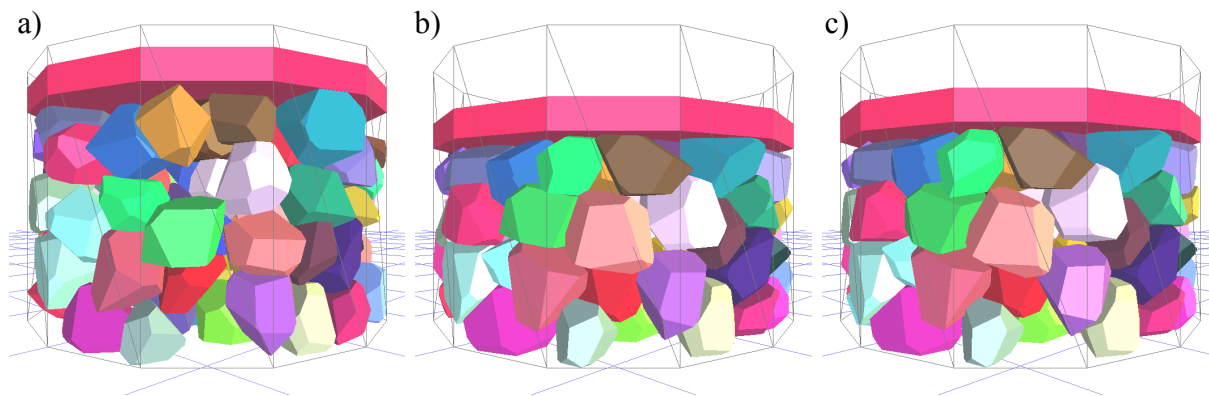|				
ballast	normal volumetric stiffness	k_{bn}	N/m^3	$1.5 \times 10^{11} - 1.5 \times 10^{13}$
	shear stiffness	k_{bs}	N/m	$k_{bn}/10^5$
	friction angle	φ_b	rad	0.6
	density	ρ_b	kg/m^3	2600
steel	normal volumetric stiffness	k_{sn}	N/m^3	$10 \times k_{bn}$
	shear stiffness	k_{ss}	N/m	$k_{sn}/10^5$
	friction angle	φ_s	rad	0.4
	density	ρ_s	kg/m^3	7800

Figure 3: Snapshots of ballast particles during simulation: a) at the beginning of loading; b) at the maximum load; c) after releasing all the load.

polyhedrons exceeding limit 0.18 m were removed, a steel loading plate was placed at the top of the granular assembly with surcharge force 250 N, the gravity and the friction angle were set to their normal values. Then, the simulation continued until low value of unbalanced forces was reached again. At that point, loading by sinusoidal wave started. Similarly to Lim and McDowell [13], the time of loading was shortened to 0.5 s.

Polyhedrons used in the simulation were generated by Voronoi tessellation. About 400 of them were successfully placed. The scaling factors s_x, s_y and s_z were chosen randomly with the uniform distribution between 30 and 45 mm and independently in all three directions. Material properties of the ballast and steel are specified in Tab. 1. Three variants differing by the normal volumetric stiffness of the ballast were considered: $k_{bn} = 1.5 \times 10^{11}$ N/m³, 1.5×10^{12} N/m³ and 1.5×10^{13} N/m³. Time step was 4.3×10^{-6}, 1.36×10^{-6} and 4.3×10^{-7} s depending on the ballast stiffness. Damping coefficient was set to 0.3.

Views of the ballast assembly at the beginning of loading, at the maximum load and after the load was released is showed in Figure 3. Since no crushing was considered at this point, the polyhedral shapes do not change. Displacement u of the steel loading plate was measured and it is plotted against the loading force in Fig. 4. Three variants of the stiffness are showed in different colors. From 2 to 4 simulations with different random seeds were calculated for each stiffness variant. The experimental measurement [13] is the bold red line. The same simulations and experiment are showed also in Fig. 5, where mean compressive stress $\sigma = -F/\pi 0.15^2$ in logarithmic scale is plotted against a relative volume change $V/V_0 = (0.15 + u)/0.15$.

Though the experimental and simulation responses are different, there is a correspondence in the unloading stiffness. For the most stiff variant with $k_{bn} = 1.5 \times 10^{13}$, the slopes of unloading curves are comparable. Loading branch cannot be correct without implementation of the crushing. Even after crushing is introduced, the achieved level of compaction in the experiment will be far from the low compaction level in the model.
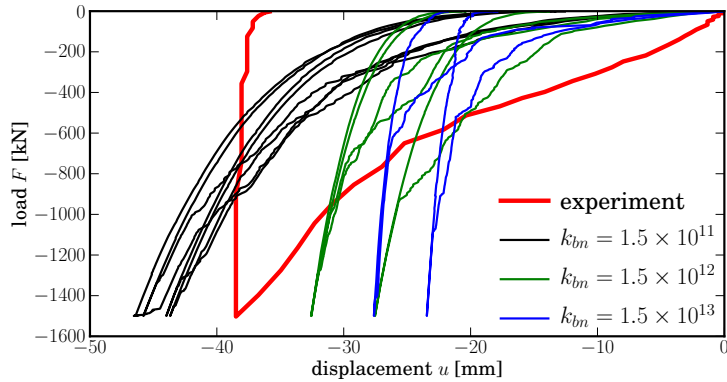
7

Figure 4: Load-displacement response of the large oedometric test and its simulations.
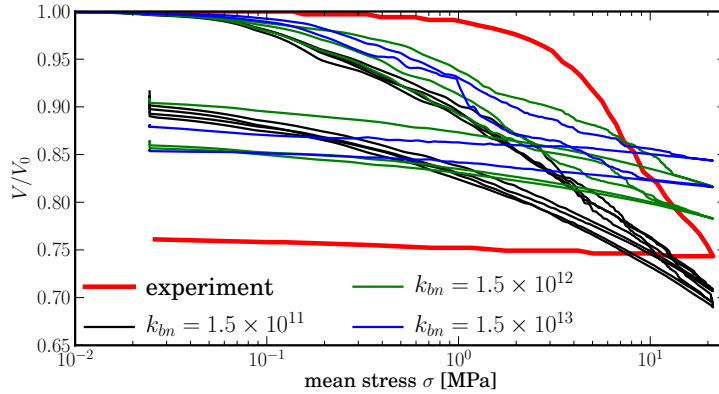

Figure 5: Mean compressive stress versus relative change in volume measured during the large oedometric test and its simulations.

The whole simulation including the free fall and two equilibrations took about 1.5, 3 or 6 days depending on the gravel stiffness. One Intel Xeon core with frequency 2.53 GHz was used.

5   CONCLUSIONS

The paper presents DEM simulation of railway ballast. Particularly, three outcomes were showed:

- A method to generate random polyhedral shapes of ballast particles using Voronoi tessellation on randomly placed nuclei. One can specify particle size and aspect ratio.

- An algorithm to estimate the repulsive force and the normal direction between two overlapping polyhedrons was developed. It is based on calculation of volumetric and surface intersections. Comparison to the standard common plane method has not been performed yet.

- The model was validated by simulation of a large oedometric test using the proposed random polyhedral shape of elements and volumetric-based contact response. No crushing was considered.

ACKNOWLEDGEMENT

References

[1] Bathurst, R. J. & L. Rothenburg (1992). Micromechanical features of granular assemblies with planar elliptical particles. *Geotechnique 42*(1), 79–95.

[2] Boon, C., G. Houlsby, & S. Utili (2012). A new algorithm for contact detection between convex polygonal and polyhedral particles in the Discrete Element Method. *Comput. Geotech. 44*, 73–82.

[3] CGAL (2013). Computational Geometry Algorithms Library. http://www.cgal.org.

[4] Cundall, P. (1988). Formulation of a three-dimensional distinct element model–Part I. a scheme to detect and represent contacts in a system composed of many polyhedral blocks. *Int. J. Rock. Mech. Min. 25*(3), 107–116.

[5] Ferellec, J.-F. & G. R. McDowell (2010). A method to model realistic particle shape and inertia in DEM. *Granular Matter. 12*(5), 459–467.

[6] Günther, O. & E. Wong (1991). A dual approach to detect polyhedral intersections in arbitrary dimensions. *BIT Numerical Mathematics 31*(1), 2–14.

[7] Hart, R., P. Cundall, & J. Lemos (1988). Formulation of a three-dimensional distinct element model–Part II. mechanical calculations for motion and interaction of a system composed of many polyhedral blocks. *Int. J. Rock. Mech. Min. 25*(3), 117–125.

[8] Höhner, D., S. Wirtz, H. Kruggel-Emden, & V. Scherer (2011). Comparison of the multi-sphere and polyhedral approach to simulate non-spherical particles within the discrete element method: Influence on temporal force evolution for multiple contacts. *Powder Technol. 208*(3), 643–656.

[9] Huang, H. (2010). *Discrete element modeling of railroad ballast using imaging based aggregate morphology characterization.* PhD, University of Illinois at Urbana-Champaign.

[10] Kettner, L. (1999). Using generic programming for designing a data structure for polyhedral surfaces. *Computational Geometry 13*(1), 65–90.

[11] Kozicki, J. & F. Donz (2008). A new open-source software developed for numerical simulations using discrete modeling methods. *Comput. Method. Appl. Mech. 197*(4950), 4429–4443.

[12] Lim, W. L. (2004). *Mechanics of railway ballast behaviour.* PhD, University of Nottingham.

[13] Lim, W. L. & G. R. McDowell (2005). Discrete element modelling of railway ballast. *Granular Matter. 7*(1), 19–29.

[14] Lobo-Guerrero, S. & L. E. Vallejo (2006). Discrete element method analysis of rail-track ballast degradation during cyclic loading. *Granular Matter. 8*(3-4), 195–204.

[15] Muller, D. E. & F. P. Preparata (1978). Finding the intersection of two convex polyhedra. *Theor. Comput. Sci. 7*, 217–236.

[16] Nezami, E. G., Y. M. Hashash, D. Zhao, & J. Ghaboussi (2004). A fast contact detection algorithm for 3-D Discrete Element Method. *Comput. Geotech. 31*(7), 575–587.

[17] Nezami, E. G., Y. M. Hashash, D. Zhao, & J. Ghaboussi (2006). Shortest link method for contact detection in Discrete Element Method. *Int. J. Numer. Anal. Met. 30*(8), 783–801.

[18] Nezami, E. G., Y. M. A. Hashash, D. Zhao, & J. Ghaboussi (2007). Simulation of front end loader bucketsoil interaction using discrete element method. *Int. J. Numer. Anal. Met. 31*(9), 11471162.

[19] Saussine, G., C. Cholet, P. Gautier, F. Dubois, C. Bohatier, & J. Moreau (2006). Modelling ballast behaviour under dynamic loading. Part 1: A 2D polygonal discrete element method approach. *Comput. Method. Appl. M. 195*(1922), 2841–2859.

[20] Song, Y., R. Turton, & F. Kayihan (2006). Contact detection algorithms for DEM simulations of tablet-shaped particles. *Powder Technol. 161*(1), 32–40.

[21] Szarf, K., G. Combe, & P. Villard (2012). Polygons vs. clumps of discs: a numerical study of the influence of grain shape on the mechanical behaviour of granular materials. *Powder Technol. 208*(2), 279–288.

[22] Tonon, F. (2004). Explicit exact formulas for the 3-D tetrahedron inertia tensor in terms of its vertex coordinates. *J. Math. Stat. 1*(1), 8–11.

[23] Šmilauer, V., E. Catalano, B. Chareyre, S. Dorofenko, J. Duriez, A. Gladky, J. Kozicki, C. Modenese, L. Scholtès, L. Sibille, J. Stránský, & K. Thoeni (2010). *Yade Documentation* (1st ed.). The Yade Project. http://yade-dem.org/doc/.